Shock Waves (2021) 31:231–238
https://doi.org/10.1007/s00193-021-01012-y

ORIGINAL ARTICLE

A new blast wave scaling

T. Wei[1] · M. J. Hargather[1]

Received: 23 July 2020 / Revised: 7 April 2021 / Accepted: 13 April 2021 / Published online: 13 May 2021

Abstract
A new scaling is developed for both air and underwater blast waves based on dimensional analysis. The new length, time, velocity, and pressure scales are based on three control parameters: the energy release of the explosive E_{HE}, the density of the undisturbed ambient medium ρ_0, and the speed of sound in the undisturbed ambient medium C_0. The shock wave propagation is divided into two regimes based on its decay characteristics, and the resulting control parameters are different in each regime. For strong shocks with Mach numbers $M_{SW} \gtrsim 5$, the increase in the shock wave radius R with time t is approximated by a power law with an exponent of $2/5$ as previously described by G. I. Taylor. Shock propagation in this regime is shown to not be a function of the ambient medium sound speed, but only the ambient medium density, explosive energy release, and time. For weak shock waves with Mach numbers $M_{SW} \lesssim 5$, the shock wave radius increase with time can be approximated by a linear function plus a logarithmic-type correction which decays to a sound wave at sufficiently long time. Shock propagation in this regime is scaled according to the medium's ambient density, sound speed, explosive energy release, and time. The new scaling is compared to, and agrees well with, published experimental data for air and underwater blasts, from milligram explosions to nuclear blasts. The new scaling improves upon traditional Hopkinson and Sachs scaling by relating shock propagation in liquid and gas environments, allowing them to be scaled to a single functional relationship. The functional scaling relationships developed here are dimensionless.

Keywords Blast wave · Scaling · Explosion

1 Introduction

Shock waves generated by explosions propagate through an ambient environment producing overpressures and ultimately damage throughout the blast field. Shock wave position versus time from explosions is one of the most fundamental measurements in explosive engineering applications and has been reported throughout the history of explosive studies [1–5]. Many experimental methodologies have been developed to identify shock wave propagation including photogrammetry [6], particle tracers [7], and refractive imaging [5,8–10], and pressure gauges as time of arrival sensors. Although many experimental approaches have been applied, theoretical prediction from first principles, i.e., governing equations, is limited, and the predictions rely heavily on experimental studies.

A powerful tool for semi-analytic analysis of blast waves is dimensional analysis, which has been applied from the beginning of blast wave studies [11,12]. Dimensional analysis is regularly incorporated in the study of fluid dynamics, heat transfer, and explosives (see, e.g., Buckingham [13], Bridgman [14], Taylor [1], Sedov [15], Baker [16], and Barenblatt [17]). According to Churchill [18], the fundamental basis for dimensional analysis was established by Fourier in 1822. Rayleigh [19] demonstrated the power of dimensional analysis in a short paper published in the *Nature* magazine in 1915, giving examples from various fields. Taylor [1] demonstrated the power of dimensional analysis in the prediction of the first atomic blast energy release using a series of pictures.

Dimensional analysis is not only useful in providing proper scaling for the experimental data, but the proper scaling can yield insight into the underlying physics. The first step in a dimensional analysis is to identify relevant parameters in the physical problem. Table 1 lists some of the major parameters that affect the propagation of shock

Communicated by C. Needham.

✉ M. J. Hargather
michael.hargather@nmt.edu

T. Wei
tie.wei@nmt.edu

[1] New Mexico Tech, Socorro, NM 87801, USA

Table 1 Parameters involved in shock wave propagation

High explosive parameters	Ambient medium parameters	Blast wave parameters
ρ_{HE}: density of HE	ρ_0: density of ambient medium	t: time of arrival
e_{HE}: specific energy of HE	C_0: speed of sound	R: shock wave location
r_{HE}: radius of HE	P_0: ambient pressure	U_{SW}: shock wave speed
s_i: shape parameters	T_0: ambient temperature	u: particle velocity
V_{det}: detonation speed	γ: adiabatic index	P_{max}: peak shock wave pressure
		I: impulse

Table 2 Traditional scaling laws of blast waves by Hopkinson–Cranz [11,12], Sachs [21], and Baker [16]

	Hopkinson–Cranz	Sachs	Baker
Repeating variables	W_{HE}	E_{HE}, ρ_0, P_0	E_{HE}, C_0, P_0
Characteristic length	$l_c \sim W_{HE}^{1/3} \sim r_{HE}$	$l_c = \left(\frac{E_{HE}}{P_0}\right)^{1/3}$	$l_c = \left(\frac{E_{HE}}{P_0}\right)^{1/3}$
Scaled distance from source	$\frac{R}{W_{HE}^{1/3}}$	$\frac{R}{l_c} = \frac{R P_0^{1/3}}{W_{HE}^{1/3}}$	$\frac{R}{l_c} = \frac{R P_0^{1/3}}{E_{HE}^{1/3}}$

waves: high explosive (HE) properties (column 1), ambient medium properties (column 2), and the shock wave properties (column 3).

Explosives are frequently characterized by their specific energy release $e_{HE} = E_{HE}/m_{HE}$. In general, the specific energy of common high explosives is similar, and the difference is rarely larger than 50%. Moreover, the difference of explosives becomes smaller when e_{HE} is raised by a 1/3 power, as shown below in the analysis. Here, the heat of detonation (e.g., $e_{HE} \approx 4.6$ MJ/kg for TNT, $e_{HE} \approx 5.81$ MJ/kg for PETN) [20] is used as the energy release for the scaling as a representative total energy release.

The first scaling of blast waves was developed more than one hundred years ago, independently by Hopkinson [11] and Cranz [12]. The Hopkinson–Cranz "law" was based on empirical observation, and the scaled distance z is still a dimensional variable:

$$z \overset{\text{def}}{=} \frac{R}{W_{HE}^{1/3}} \tag{1}$$

where R is the distance from the detonation center and W_{HE} is the weight of the explosive. Thus, the Hopkinson–Cranz law is also called the cube-root law. The Hopkinson–Cranz law which states that similar shock waves are generated from two explosions at the same scaled distance z is convenient in many practical applications. A shortcoming of the Hopkinson–Cranz law is that the ambient mediums for the two explosions have to be at the same conditions.

In the 1940s, Sachs [21] improved the Hopkinson–Cranz law by considering the effect of the external atmospheric conditions. Using a similarity transformation, Sachs derived a scaling that accounts for the effects of atmospheric conditions. Sachs scaling can be presented as:

$$z \overset{\text{def}}{=} \frac{R P_0^{1/3}}{W_{HE}^{1/3}} \tag{2}$$

A formal dimensional analysis of shock waves was performed by Baker et al. [16], who chose E_{HE}, P_0, and C_0 as the repeating variables.

The traditional scaling relations of shock wave are summarized in Table 2. In the traditional analysis, the air blast and underwater blasts are typically treated separately. In the present work, a unified scaling is developed for air and underwater blasts from a dimensional analysis.

2 New shock wave scaling

Proper selection of control parameters is of utmost importance in a successful dimensional analysis of any flow or heat transport problem. Here, a dimensional analysis, differing from that of Baker's by the selection of the control parameters, is proposed. The control parameters are selected as E_{HE}, ρ_0, C_0, and the independent variable is the shock wave arrival time t. The new dimensional analysis is summarized in Table 3, where the third row is the non-dimensional control parameter of the problem. In the new dimensional analysis, there are four control parameters, entailing three primary dimensions: mass, length, and time. Thus, there is only one non-dimensional control parameter, Π_t.

In this scaling analysis, the velocity scale is set as C_0 or the speed of sound in the undisturbed ambient medium. The length scale is set as:

$$l_c \overset{\text{def}}{=} \left(\frac{E_{HE}}{\rho_0 C_0^2}\right)^{1/3} = (\Psi_{HE})^{1/3} \left(\frac{\rho_{HE} e_{HE}}{\rho_0 C_0^2}\right)^{1/3} \tag{3}$$

Table 3 New dimensional analysis of blast wave

Control parameters	$E_{\mathrm{HE}},\ \rho_0,\ C_0,\ t$
Repeating variables	$E_{\mathrm{HE}},\ \rho_0,\ C_0$
Non-dimensional control parameter, Π	$\Pi_t = \frac{t\ C_0}{(E_{\mathrm{HE}}/(\rho_0 C_0^2))^{1/3}}$
Characteristic length	$l_{\mathrm{c}} \stackrel{\mathrm{def}}{=} \left(\frac{E_{\mathrm{HE}}}{\rho_0 C_0^2}\right)^{1/3}$

Hence, the length scale l_{c} is directly related to the property of the explosive (E_{HE}) and the ambient medium (ρ_0 and C_0). Equation (3) shows that l_{c} is proportional to the radius of the high explosive, r_{HE}, via the volume $\mathcal{V}_{\mathrm{HE}}$. As an example, for a spherical shape HE, $(\mathcal{V}_{\mathrm{HE}})^{1/3} = 1.61 r_{\mathrm{HE}}$. Equation (3) also shows that l_{c} is proportional to the ratio $(\rho_{\mathrm{HE}}\, e_{\mathrm{HE}}/(\rho_0\, C_0^2))^{1/3}$, where $\rho_{\mathrm{HE}}\, e_{\mathrm{HE}}$ is the energy of the high explosive per unit volume and $\rho_0\, C_0^2$ is the kinetic energy of the ambient medium moving at the speed of sound. For TNT blast in air, $(\rho_{\mathrm{HE}}\, e_{\mathrm{HE}}/(\rho_0\, C_0^2))^{1/3} \approx 38.5$, and for TNT blast under water, $(\rho_{\mathrm{HE}}\, e_{\mathrm{HE}}/(\rho_0\, C_0^2))^{1/3} \approx 1.5$. This ratio is much larger than 1 for a nuclear blast.

The time scale is set as:

$$t_{\mathrm{c}} \stackrel{\mathrm{def}}{=} \frac{l_{\mathrm{c}}}{C_0} \tag{4}$$

Thus, the time scale also depends on both the explosive properties and the ambient medium properties. The pressure scale is set as

$$P_{\mathrm{c}} \stackrel{\mathrm{def}}{=} \rho_0 C_0^2 \tag{5}$$

The pressure scale depends solely on the properties of the ambient medium.

A dimensional analysis for the shock wave radius growth with time can be presented as:

$$R = f(E_{\mathrm{HE}}, \rho_0, C_0, t) \tag{6}$$

and the new non-dimensional, scaled variables are denoted by a superscript * as:

$$R^* \stackrel{\mathrm{def}}{=} \frac{R}{l_{\mathrm{c}}} = \frac{R}{(E_{\mathrm{HE}}/(\rho_0 C_0^2))^{1/3}} = \frac{R}{m_{\mathrm{HE}}^{1/3}} \frac{(\rho_0 C_0^2)^{1/3}}{e_{\mathrm{HE}}^{1/3}} \tag{7a}$$

$$t^* \stackrel{\mathrm{def}}{=} \frac{t}{t_{\mathrm{c}}} = \frac{t\ C_0}{(E_{\mathrm{HE}}/(\rho_0 C_0^2))^{1/3}} \tag{7b}$$

Thus, the non-dimensional form for the growth of shock wave radius is given by:

$$R^* = \Psi_1(t^*) \tag{8}$$

where Ψ_1 is a non-dimensional function that needs to be determined from experimental measurements or numerical simulation, or if possible, from an analytic solution.

Examining (7a), the Hopkinson–Cranz scaled distance $z = R/W_{\mathrm{HE}}^{1/3}$ is one part of the new scaled distance. The second part is an atmospheric scaling, which is similar to the Sachs scaling, but uses an atmospheric dynamic pressure based on sound speed instead of static atmospheric pressure. If the ambient medium is a gas, then $\rho_0 C_0^2 = \gamma\ P_0$, and the new scaled shock wave radius can be written as:

$$R^* = \frac{R P_0^{1/3}}{m_{\mathrm{HE}}^{1/3}} \frac{\gamma^{1/3}}{e_{\mathrm{HE}}^{1/3}} \tag{9}$$

This reproduces the Sachs scaled distance (Table 2). However, Sachs scaling cannot be applied to the underwater blast. The new scaling applies to both air and underwater blasts.

Similarly, a dimensional analysis for the pressure of the shock wave can be presented as:

$$P = f(E_{\mathrm{HE}}, \rho_0, C_0, t) \tag{10}$$

Denoting the scaled, non-dimensional pressure as $P^* \stackrel{\mathrm{def}}{=} P/(\rho_0 C_0^2)$, the non-dimensional pressure can be presented as

$$P^* = \Psi_2(t^*) \tag{11}$$

where the non-dimensional function also needs to be determined by experimental, numerical, or analytical solution.

The shock wave radius R can also be used as the independent variable, instead of the arrival time t. For example, the dimensional analysis for pressure or overpressure can also be presented as:

$$P = f(E_{\mathrm{HE}}, \rho_0, C_0, R) \tag{12}$$

and the non-dimensional form becomes

$$P^* = \Psi_3(R^*) \tag{13}$$

The non-dimensional form of pressure as a function of radius is generally more useful for explosive applications and is used here for comparison with experimental data.

3 Scaling of the shock wave radius

This scaling and dimensional analysis is evaluated here using published experimental measurements of shock wave propagation from numerous sources. Figure 1a presents the dimensional shock wave radius versus the dimensional arrival time. The data include air and underwater blasts of explosions from milligrams to 100 ton, as well as nuclear blasts. The measured times range from 0.1 μs to 1 s, and the shock wave radius ranges from 1 mm to 1 km.

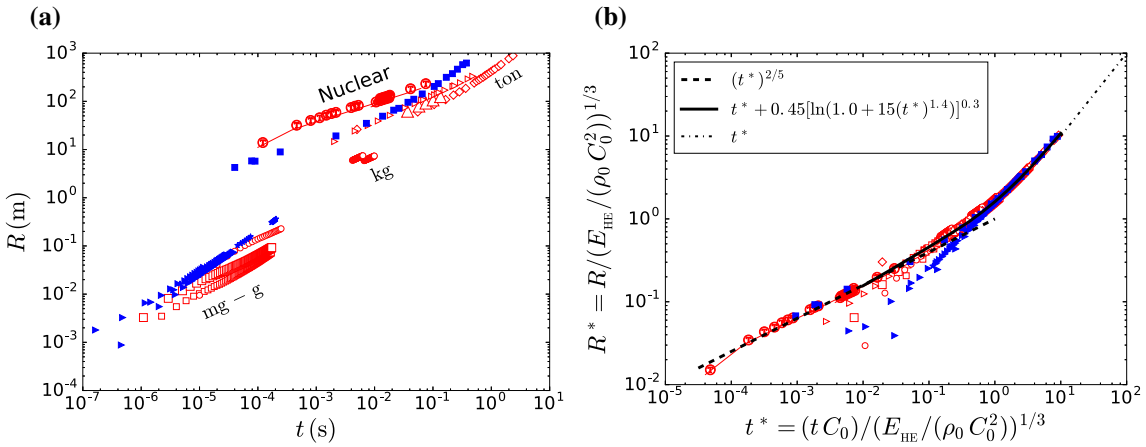

Fig. 1 **a** Dimensional shock wave radius versus time. Red open symbols are air blast, and filled blue symbols are underwater blast. **b** Scaled shock wave radius and arrival time, R^* versus t^*, using new scaling

In Fig. 1a, the air blast data with small t and R include experiments of Kleine [8] (milligrams of AgN_3) and Hargather and Settles [9] (grams of PETN). The kilogram C4 air blast data are from Hargather [10] . The 100 ton TNT blast data are from Kingery et al. [3], and 20 ton propane blast data are from Dewey [22]. The nuclear blast data include Trinity [1], Grable, and MET [23]. The underwater blast data presented in Fig. 1a are from Itoh et al. [24] (0.1 kg SEP), Kira et al. [25] (0.005−0.1 kg SEP), and a nuclear blast published by Porzel [26].

Figure 1b presents the new scaled shock wave radius versus the new scaled time: R^* versus t^*. Overall, the new scaling collapses the air and underwater blast data well. Scatter is observed in the near charge measurements of small scale explosions. It is known that the traditional scaling laws are most improbable near the charge surface [2]. Possible causes of the scatter near the charge surface include that the radius of shock wave immediately after detonation is affected by the shape of the explosive, the actual detonation is not instantaneous, and experimental measurement uncertainties are higher in regions of high shock wave velocities.

Based on the characteristics of shock wave radius growth with time shown in Fig. 1b, the propagation of a shock wave can be divided into two regimes: strong and weak shock waves. For strong shock waves (small t^*, or small R^* and large M_{SW}), the growth of the shock wave radius with time can be approximated as:

$$R^* \approx (t^*)^{2/5} \quad \text{for} \quad M_{SW} \gtrsim 5 \tag{14}$$

The 2/5 power law was first derived by Taylor [1], von Neumann [27], and Sedov [15]. According to von Neumann [27], the 2/5 power law was presented by G. I. Taylor in June 27, 1941 (British Report RC-210), and by J. von Neumann in June 30, 1941 (NDRC, Div. B, Report AM-9). G. I. Taylor applied a classic dimensional analysis, and von Neumann's arguments were also essentially dimensional analysis. Sedov's derivation was based on a similarity solution (see, e.g., [28]). As the exponent 2/5 was first suggested by Taylor [1], this region is referred to as the Taylor regime or the strong shock regime. The shock wave Mach number in the Taylor regime can be approximated as:

$$M_{SW} \approx \frac{2}{5}(t^*)^{-3/5} \approx \frac{2}{5}(R^*)^{-3/2} \quad \text{for} \quad M_{SW} \gtrsim 5 \tag{15}$$

For smaller shock wave Mach numbers ($M_{SW} \lesssim 5$), termed the weak shock regime, the growth of the shock wave radius can be approximated as:

$$R^* \approx t^* + a\left[\ln(b + c(t^*)^m)\right]^n \quad \text{for} \quad M_{SW} \lesssim 5 \tag{16}$$

where the coefficient b is assigned to be 1 to match the origin ($R^* = 0$ at $t^* = 0$) and coefficients a, c, m, and n are determined by curve fitting. Using the experimental data, here the values of $a \approx 0.45$, $c \approx 15$, $m = 1.4$, and $n \approx 0.3$ were found. These coefficients or the function form for the weak shock regime are in no sense exact. More data are required to improve determination of the coefficients and to potentially identify more physically fundamental functions. Logarithmic-type functions have been used in previous studies of weak shock waves, but are not identified via an analytical solution of the problem. For example, Kirkwood and Brinkley [29] derived an asymptotic function at large distances, in which the maximum pressure is proportional to the inverse of the logarithmic of the shock radius. Based on curve fitting, Goodman developed a formula for the maximum overpressure at large distance [2] and a logarithmic function is involved. Dewey [7] has also proposed an empirical function that uses logarithmic functions which has been widely used in recent studies [5,9,10], but the functional form can result in unphysical values if extrapolated outside the data used for the

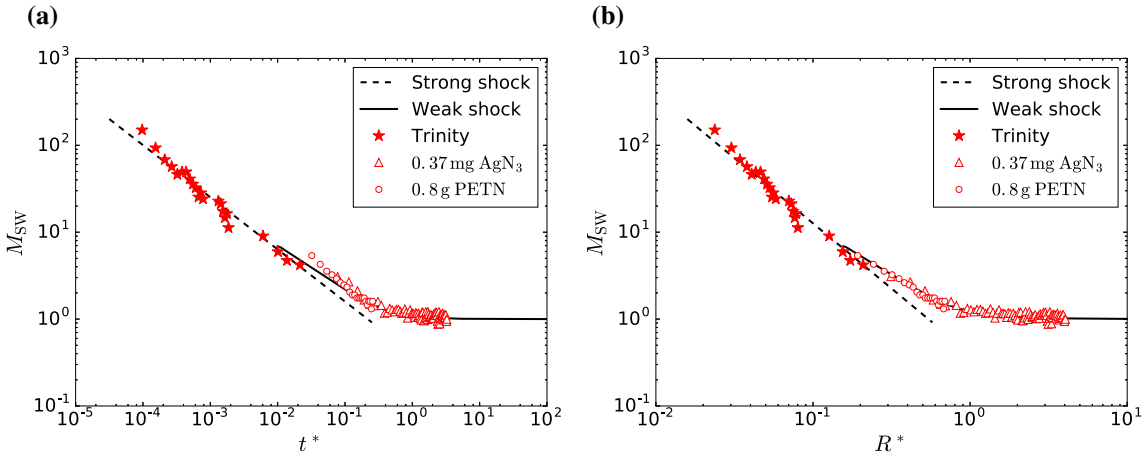

Fig. 2 The predicted shock wave Mach numbers for the strong shock regime (15) and the weak shock regime (17). **a** Shock wave Mach number versus the scaled time. **b** Shock wave Mach number versus the scaled radius. To avoid clutter, only three data are shown including the Trinity nuclear blast, 0.37 mg AgN_3 (silver azide) data are from Kleine [8], and the 0.8 g PETN data are from Hargather and Settles [9]

Table 4 Regimes in the propagation of a shock wave

Strong shock regime	Weak shock regime
$t^* \lesssim 0.02$	$t^* \gtrsim 0.02$
$R^* \lesssim 0.2$	$R^* \gtrsim 0.2$
$M_{sw} \gtrsim 5$	$M_{sw} \lesssim 5$
$R^* \sim (t^*)^{2/5}$	$R^* \sim t^* + a\left[\ln(b + c(t^*)^m)\right]^n$
	$a = 0.45, b = 1, c = 15, m = 1.4, n = 0.3$
$M_{sw} \approx (2/5)(t^*)^{-3/5} \approx (2/5)(R^*)^{-3/2}$	$M_{SW} \approx 1 + \frac{a \cdot c \cdot m \cdot n\,(t^*)^{m-1}}{(b+c(t^*)^m)\left[\ln(b+c(t^*)^m)\right]^{1-n}}$

fit. The form proposed by Dewey is a dimensional equation, for which each of the four curve fit coefficients has a different dimensional value. The scaling relationship proposed here in (16) is completely dimensionless, and all of the coefficients are also dimensionless.

The shock wave Mach number in the weak shock regime can be expressed by differentiating (16):

$$M_{SW} \approx 1 + \frac{a \cdot c \cdot m \cdot n \cdot (t^*)^{m-1}}{(b + c(t^*)^m)\left[\ln(b + c(t^*)^m)\right]^{1-n}} \quad \text{for} \quad M_{SW} \lesssim 5 \tag{17}$$

Thus, the shock wave propagation in the weak shock regime is approximated by a sound wave plus a logarithmic correction. As $t^* \to \infty$, the Mach number approaches 1, as physically expected.

The predicted shock wave Mach numbers for the strong shock regime and the weak shock regime are illustrated in Fig. 2. To avoid clutter, only three data sets of shock wave Mach number are presented in the figure. The shock Mach number M_{SW} is computed by finite differencing of the measurement shock wave radius data. Overall, (15) and (17) agree reasonably well with the experimental data.

4 Control parameters in different regimes

Experimental data shown in the preceding sections indicate that the propagation of shock waves can be divided into two regimes: a strong shock regime and a weak shock regime, which decays to a sound wave. In the strong shock regime, the shock wave radius grows with time as a 2/5 power law.

In G. I. Taylor's dimensional analysis, the control parameters for the shock wave radius are given as

$$R = f(E_{HE}, \rho_0, t) \tag{18}$$

Compared with (6), Taylor's dimensional analysis did not include the speed of sound as a control parameter, which leads directly to a 2/5 power law with time.

In the strong shock regime, the sound speed of the undisturbed medium C_0 is not a control parameter, because the shock velocity is much larger than C_0. However, as the shock decays and its velocity becomes comparable with the sound speed, C_0 becomes an important control parameter. As shock wave decays further, the energy release of the high explosive, E_{HE}, becomes irrelevant and the shock wave transitions to a sound wave. The control parameters are summarized in Table 5 for the strong and weak regimes. Table 5 also shows

Table 5 Control parameters in different regimes of shock wave propagation

Regime	Strong shock	Weak shock	Sound wave
t^*	$t^* \lesssim 0.05$	$0.05 \lesssim t^* \lesssim 1$	$t^* \gtrsim 1$
Control parameters	$t;\ E_{\mathrm{HE}}, \rho_0$	$t;\ E_{\mathrm{HE}}, \rho_0, C_0$	$t;\ \rho_0, C_0$
M_{SW}	$(2/5)(t^*)^{-3/5}$	$\Psi(t^*)$	1

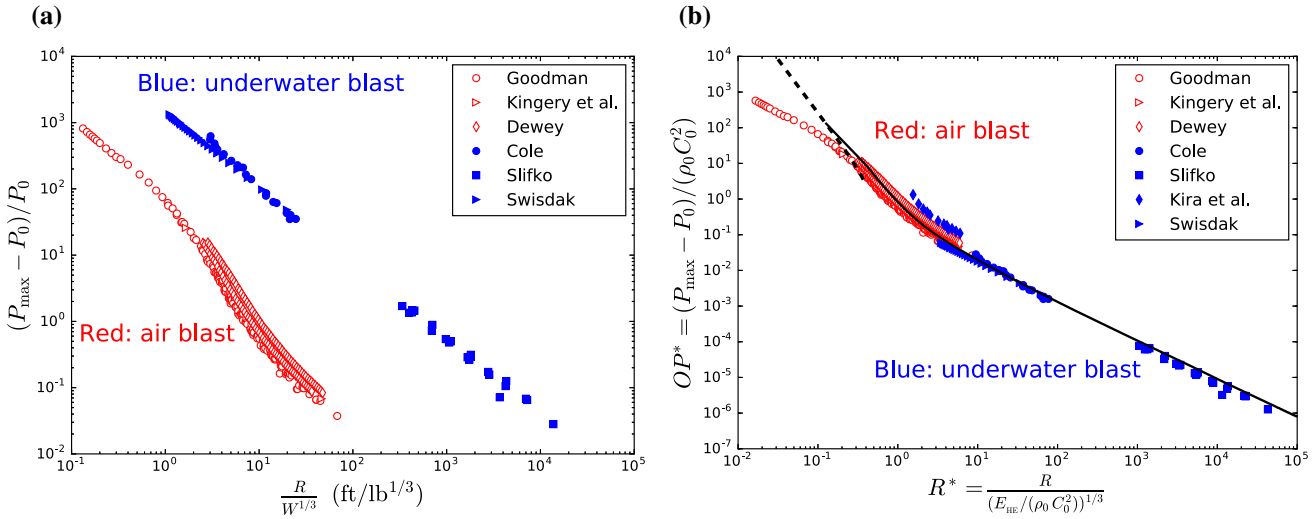

Fig. 3 Scaling of the maximum overpressure in air blast and underwater blast: **a** Hopkinson–Cranz scaling, **b** new scaling. The dashed curve for $R^* < 0.3$ in Fig. 3b represents (20) with M_{SW} approximated by (15), and the solid curve for $R^* > 1$ in Fig. 3b represents (20) with M_{SW} approximated by (17). The sources of the air blasts are [2,3,22], and the sources of the underwater blast are [25,32–34]

the control parameters for a sound wave, which is the limit of the weak shock wave regime.

5 Scaling of the peak overpressure

Overpressure is one of the most important quantities in the study of shock waves. Overpressure (OP) represents the pressure rise over atmospheric pressure that occurs as a shock wave propagates past a location of interest [30]. The overpressure integrated over time represents the explosive impulse, which describes a structure's response to shock loading [30]. The peak overpressure produced by a shock wave in a gas can be calculated from the shock wave Mach number at a given location using one-dimensional gas dynamics relationships:

$$\frac{\mathrm{OP}_{\max}}{P_0} \approx \frac{2\gamma}{\gamma+1}(M_{\mathrm{SW}}^2 - 1) \tag{19}$$

which has been shown to be accurate for a range of charge sizes [5,9,10,30,31]. The overpressure thus scales with the shock wave Mach number. Figure 3a presents the overpressure versus the distance using the traditional Hopkinson–Cranz's scaling. The air blast and underwater blast data collapse individually to two separate curves. The new scaling developed here scales overpressure according to:

$$\frac{\mathrm{OP}_{\max}}{\rho_0 C_0^2} \approx \frac{2\gamma^2}{\gamma+1}(M_{\mathrm{SW}}^2 - 1) \tag{20}$$

In Fig. 3b, the new scaling is applied to the overpressure and the distance from the detonation center which collapses the air blast and underwater blast onto one curve. The dashed curve for $R^* < 0.2$ in Fig. 3b represents (20) with M_{SW} approximated by (15), and the solid curve in Fig. 3b represents (20) with M_{SW} approximated by (17). Note that deviation from the curve at small radii and high pressure are due to the failure of the ideal gas law assumptions built into (19).

6 Conclusions

A new dimensional analysis was developed to study the propagation of shock waves. The new analysis unifies the scaling for the air blasts and underwater blasts through the definition of new length, time, and pressure scales. The shock wave

propagation is divided into strong shock and weak shock regimes based on the shock wave Mach number, observed growth characteristics, and relative importance of identified control parameters. The control parameters in this new dimensional analysis are the energy release of the explosion E_{HE}, the density of the ambient medium ρ_0, and the speed of sound in the undisturbed ambient medium C_0.

Dimensionless functional relationships for the shock wave growth are developed here. At large shock wave Mach number, $M_{sw} \gtrsim 5$, the growth of the shock wave radius is proportional to $t^{2/5}$ which agrees with the analytical solutions developed by G. I. Taylor and others. Shock propagation in this regime is shown to not be a function of the ambient medium sound speed, but only the ambient medium density, explosive energy release, and time. For weak shock waves with Mach numbers $M_{SW} \lesssim 5$, the shock wave radius increase with time can be approximated by a linear function plus a logarithmic-type correction which decays to a sound wave at sufficiently long time. Shock propagation in this regime is scaled according to medium's ambient density, sound speed, explosive energy release, and time. The identification of these control parameters in each shock wave regime has not been previously reported.

The new scaling collapses well the experimental data of the shock wave radius and overpressure from both air blasts and underwater blasts across many orders of magnitude, from milligrams to kiloton explosive charge masses.

Acknowledgements Portions of this work were funded by DTRA grant HDTRA1-18-1-0022.

References

1. Taylor, G.I.: The formation of a blast wave by a very intense explosion. II. The atomic explosion of 1945. Proc. R. Soc. Lond. Ser. A Math. Phys. Sci. **201**(1065), 175–186 (1950). https://doi.org/10.1098/rspa.1950.0050
2. Goodman, H.J.: Compiled free-air blast data on bare spherical pentolite. Technical Report 1092, Ballistic Research Laboratory (1960)
3. Kingery, C.N., Keefer, J.H., Day, J.D.: Surface air blast measurements from a 100-ton TNT detonation. Technical Report 1410, Ballistic Research Laboratory (1962)
4. Dewey, J.M.: Expanding spherical shocks (blast waves). In: Ben-Dor, G., Igra, O., Elperin, E. (eds.) Handbook of Shock Waves, vol. 2, pp. 441–481. Academic Press, San Diego (2001)
5. Kleine, H., Dewey, J.M., Ohashi, K., Mizukaki, T., Takayama, K.: Studies of the TNT equivalence of silver azide charges. Shock Waves **13**(2), 123–138 (2003). https://doi.org/10.1007/s00193-003-0204-3
6. Dewey, J.M., McMillin, D.J., Classen, D.F.: Photogrammetry of spherical shocks reflected from real and ideal surfaces. J. Fluid Mech. **81**, 701–717 (1977). https://doi.org/10.1017/S0022112077002304
7. Dewey, J.M.: The properties of a blast wave obtained from an analysis of the particle trajectories. Proc. R. Soc. Lond. Ser. A Math. Phys. Sci. **324**(1558), 275–299 (1971). https://doi.org/10.1098/rspa.1971.0140
8. Kleine, H.: Filming the invisible-time-resolved visualization of compressible flows. Eur. Phys. J. Spec. Top. **182**(1), 3–34 (2010). https://doi.org/10.1140/epjst/e2010-01223-2
9. Hargather, M.J., Settles, G.S.: Optical measurement and scaling of blasts from gram-range explosive charges. Shock Waves **17**(4), 215–223 (2007). https://doi.org/10.1007/s00193-007-0108-8
10. Hargather, M.J.: Background-oriented schlieren diagnostics for large-scale explosive testing. Shock Waves **23**(5), 529–536 (2013). https://doi.org/10.1007/s00193-013-0446-7
11. Hopkinson, B.: British ordnance board minutes 13565. The National Archives, Kew, UK 11 (1915)
12. Cranz, K.J.: Lehrbuch der Ballistik. Springer, Berlin (1936)
13. Buckingham, E.: The principle of similitude. Nature **96**(2406), 396–397 (1915). https://doi.org/10.1038/096396d0
14. Bridgman, P.W.: Dimensional Analysis. Yale University Press, London (1922)
15. Sedov, L.I.: Similarity and Dimensional Methods in Mechanics. CRC Press, Boca Raton (1959)
16. Baker, W.E., Westine, P.S., Dodge, F.T.: Similarity Methods in Engineering Dynamics: Theory and Practice of Scale Modeling. Spartan Books (1973)
17. Barenblatt, G.I.: Dimensional Analysis. Gordon and Breach Science Publisher, New York (1987)
18. Churchill, S.W.: Turbulent flow and convection: the prediction of turbulent flow and convection in a round tube. Adv. Heat Transf. **34**, 255–361 (2001). https://doi.org/10.1016/S0065-2717(01)80013-7
19. Rayleigh, L.: The principle of similitude. Nature **95**, 66–68 (1915). https://doi.org/10.1038/095066c0
20. Cooper, P.: W: Explosives Engineering. Wiley-VCH, Hoboken (1996)
21. Sachs, R.G.: The dependence of blast on ambient pressure and temperature. Technical Report 466, Ballistic Research Laboratories (1944)
22. Dewey, J.M.: The TNT equivalence of an optimum propane–oxygen mixture. J. Phys. D Appl. Phys. **38**(23), 4245 (2005). https://doi.org/10.1088/0022-3727/38/23/017
23. Schmitt, D.T.: Position and volume estimation of atmospheric nuclear detonations from video reconstruction. PhD Thesis, Air Force Institute of Technology (2016)
24. Itoh, S., Hamashima, H., Murata, K., Kato, Y.: Determination of JWL parameters from underwater explosion test. 12th International Detonation Symposium, vol. 281 (2002)
25. Kira, A., Fujita, M., Itoh, S.: Underwater explosion of spherical explosives. J. Mater. Process. Technol. **85**(1–3), 64–68 (1999). https://doi.org/10.1016/S0924-0136(98)00257-X
26. Porzel, F.: Close-in time of arrival of underwater shock wave. Technical Report AD-361919, IIT Research Institute (1957)
27. Bethe, H.A., Fuchs, K., Hirschfelder, J.O., Magee, J.L., von Neumann, R.: Blast wave. Technical Report LA-2000, Los Alamos Scientific Laboratory (1947)
28. Kamm, J.R.: Evaluation of the Sedov–von Neumann–Taylor blast wave solution. Technical Report LA-UR-00-6055, Los Alamos National Laboratory (2000)
29. Brinkley Jr., S.R., Kirkwood, J.G.: Theory of the propagation of shock waves. Phys. Rev. **71**(9), 606 (1947). https://doi.org/10.1103/PhysRev.72.1109
30. Kinney, G.F., Graham, K.J.: Explosive Shocks in Air. Springer, Berlin (1985)
31. Dewey, J.M.: Measurement of the physical properties of blast waves. In: Igra, O., Seiler, F. (eds.) Experimental Methods of Shock Wave Research, pp. 53–86. Springer, Berlin (2016). https://doi.org/10.1007/978-3-319-23745-9
32. Cole, R.H.: Underwater Explosions. Princeton University Press, Princeton (1948)

33. Slifko, J.F.: Pressure-pulse characteristics of deep explosions as functions of depth and range. Technical Report 67-87, Naval Ordnance Laboratory (1967)
34. Swisdak Jr., M.M.: Explosion effects and properties. Part II. Explosion effects in water. Technical Report 76-116, Naval Surface Weapons Center, White Oak Laboratory (1978)